Ultrasound-induced mechanical damage of cancer cell cytoskeleton causes disruption of nuclear envelope and activation of cGAS-STING signaling
–Supplementary Information–

Giorgia Federico[1], Angelo Rosario Carotenuto[2,3], Arsenio Cutolo[2,3], Stefania Palumbo[2,3], Marialuisa Moccia[4], Simona Paladino[1], Massimo Santoro[1], Tommaso Russo[1], Massimiliano Fraldi[2,3,5*], and Francesca Carlomagno[1,*]

[1]Department of Molecular Medicine and Medical Biotechnologies, University of Naples "Federico II", Napoli, Italy;
[2]Department of Structures for Engineering and Architecture, University of Naples "Federico II", Napoli, Italy;
[3]Laboratory of Integrated Mechanics and Imaging for Testing and Simulation (LIMITS), University of Naples "Federico II", Napoli, Italy;
[4]Institute for the Experimental Endocrinology and Oncology "G. Salvatore", National Council of Research, Napoli, Italy;
[5]LPENS - Départment de Physique, Ecole Normale Supérieure, Paris, France;
[*]Corresponding authors: fraldi@unina.it, francesca.carlomagno@unina.it

Post-processing of AFM data and morpho-mechanical characterization of single cells

AFM investigations on cells give detailed information about the overall morphology of the cell, in terms of height maps and shape, as well as about the local mechanical properties. Repeated indentation tests let indeed to obtain a point-by-point mapping of the stiffness and Young modulus of the cells, automatically estimated by resorting to well-established results of contact mechanics. However, the outcomes of the AFM scannings return effective measurements of the mechanical properties of the target substrate when it is probed by the AFM tip. With the aim to characterize the in-frequency response of a single-cell by highlighting the behaviour of its main sub-structures, there is the need to somehow deduce from these homogenized quantities both the stiffness of the nucleus and of the surrounding cellular structures. To this scope, we exploited local properties by combining the positional and mechanical response to indentation in order to identify the stiffness constants to be uploaded in the dynamical model. Starting from AFM measurements, the height and stiffness maps have been collected and characteristic height and stiffness profiles have been reconstructed along two preferred (orthogonal) directions, selected by starting from lines intercepting the maximum height point of the cell (see Figure 1B). From such projections, smoothed profiles of the cell as well as estimations of the nuclear shape have been reconstructed, in this way identifying a central nuclear region composed by an ellipsoidal nucleus with the surrounding cytological material. More in detail, for each projection, after detecting the limiting points and the position of the nucleus, the cell height points have been interpolated by using a Gaussian-type function $f_c(s)$ with equation:

$$f_c^{(j)}(s) = h_0 + (H_m - h_0)\,\exp\left[-\frac{(s - s_n^{(j)})^2}{2\sigma_j^2}\right] \tag{S.1}$$

where s denotes the abscissa along the $j-th$ projection chord, h_0 and H_m are respectively the background and the (measured) maximum heights, while $s_n^{(j)}$ is the location of the nucleus along the line and σ_j is a shape parameter allowing for determining the adhesion spreading of the cultured cell. The difference $H_m - h_0$ returns an effective height h_{eff} for the cell. Two limiting (adhesion) points of the cell functions $\{s_1^{(j)}, s_2^{(j)}\}$ were evaluated by direct comparison with the stiffness data, in particular by detecting when the stiffness approached a threshold value indicating the transition to the external background stiffness of the substrate. Then, in order to obtain information about the nuclear morphology, we adopt an elliptical parametrization with equation:

$$f_n^{(j)}(s) = \frac{h_n}{2}\left[1 \pm \sqrt{1 - \frac{(s - s_n^{(j)})^2}{{b_n^{(j)}}^2}}\right] \tag{S.2}$$

in which h_n is a (unique) nucleus height parameter whereas $b_n^{(j)}$ represents the semi-diameter of the elliptical nucleus along the j-th chord. To estimate these two parameters of the nucleus, we then imposed that the upper part of the nucleus is in substantial contact with the cell profile at an (unknown) coordinate $s_c = s_n^{(j)} + \delta_c^{(j)}$ (symmetry of the functions let to neglect the other side), herein being also tangent each other by so simulating the adherence between cell nucleus and cytoskeletal fibers. After posing $f_{c/0}^{(j)}(s) = f_c^{(j)}(s) - h_0$, few manipulations lead to express the above mentioned requirements through the following square conditions:

$$\begin{cases} d(h_n, b_n^{(j)}, \delta_c^{(j)}) = \left|\left| f_{c/0}^{(j)}(s_c) - \frac{h_n}{2}\left[1 \pm \sqrt{1 - \frac{\delta_c^{(j)2}}{b_n^{(j)2}}}\right]\right|\right|^2 \\ \theta(h_n, b_n^{(j)}, \delta_c^{(j)}) = \left|\left| \frac{1}{\sigma_j^2} f_{c/0}^{(j)}(s_c)(f_{c/0}^{(j)}(s_c) - \frac{h_n}{2}) - \frac{h_n^2}{4b_n^{(j)2}}\right|\right|^2 \end{cases} \tag{S.3}$$

Therefore, to estimate the unknown parameters, we numerically imposed the minimization of the two congruence conditions by requiring

$$\{\tilde{h}_n, \tilde{b}_n^{(j)}, \tilde{\delta}_c^{(j)}\} : \min_{\{h_n, b_n^{(j)}, \delta_c^{(j)}\}} \left[d(h_n, b_n^{(j)}, \delta_c^{(j)}) + (s_n^{(j)} + \delta_c^{(j)})^2 \theta(h_n, b_n^{(j)}, \delta_c^{(j)}) \right] \tag{S.4}$$

under the constraints $0 < h_n < h_{eff}$, $\delta_c^{(j)} < b_n^{(j)}$ and $0 < b_n^{(j)} < 2\sigma_j^2$. The minimization returns a guess for the regularized shape of the nucleus, and in particular identifies the interval of the intracellular region occupied by the nucleus. Note that congruence requirements lead to consider, in the second projection (and in general, in the other possible trajectories passing from the maximum point), that the cell must exhibit the same effective height h_{eff}. Thus, the other fitting procedures only involve the respective width parameters σ_l, with $l \neq j$. Furthermore, the similarity among the considered regularizing functions let to simplify the geometric identification procedure by assuming that $b_n^{(l)} = \eta_{lj}\, b_n^{(j)}$, with $\eta_{lj} = \sigma_l/\sigma_j$. The estimated nuclear shape then defines a central region where the average stiffness is read from AFM data, namely $\overline{K}_{nc}^{int}$. For each projection, by posing $z = s + s_n^{(j)}$ for convenience, the average stiffness in the internal nuclear core $\overline{K}_{nc}^{int}$ can be first evaluated starting from the interpolated AFM profile as:

$$\overline{K}_{nc}^{int,j} = \frac{1}{2b_n^{(j)}} \int_{-b_n^{(j)}}^{b_n^{(j)}} K_{AFM}^{(j)}(z)\, dz \tag{S.5}$$

According to Popov's analogy describing the substrate as a spring foundation, the obtained homogenized stiffness can be therein interpreted as a Reuss combination of the nucleus and the perinuclear cytoplasm stiffness springs, i.e. $\overline{K}_{nc}^{int} = \left[\overline{K}_n^{-1} + \left(\overline{K}_c^{int}\right)^{-1}\right]^{-1}$ (see Figure 1C). Therefore, there is the practical need to discriminate between the nuclear and cellular stiffness in this region by starting from the overall experimental measurements. For the j-th projection, one has

$$\overline{K}_{nc}^{int,j} = \frac{\overline{K}_n^j\, \overline{K}_c^{int,j}}{\overline{K}_n^j + \overline{K}_c^{int,j}} \tag{S.6}$$

More specifically, in such a relationship the stiffness contribution of cytoplasm/cytoskeleton $\overline{K}_c^{int,j}$ that constitutes the nuclear envelope can be written as the ratio of an axial modulus $\overline{E_c\, A_c}$ and an intrinsic height $\overline{h}_c^{int,j}$, i.e. $\overline{K}_c^{int,j} = \overline{E_c\, A_c}/\overline{h}_c^{int,j}$. In order to estimate this medium stiffness, the two latter parameters have to be determined. To this aim, the geometric coefficient $\overline{h}_c^{int,j}$ can be obtained from the regularized cell and nucleus profiles. More specifically, equations (S.1),(S.2) and (S.4) let to define:

$$\overline{h}_c^{int,j} = \frac{1}{2\tilde{b}_n^{(j)}} \int_{-\tilde{b}_n^{(j)}}^{\tilde{b}_n^{(j)}} \| f_{c/0}^{(j)}(z) - \tilde{h}_n \sqrt{1 - \left(\frac{z}{\tilde{b}_n^{(j)}}\right)^2} \|\, dz \tag{S.7}$$

On the other hand, the axial modulus $\overline{E_c\, A_c}$ is assumed as a not region-specific term, i.e. one assumes that the Young modulus of the sole cytoplasm/cytoskeletal material (whose magnitude also accounts for the overall internal pre-stretch accumulated by the cytoskeleton in adherent configuration) and the contact area of the AFM tip do not significantly change passing from the nuclear to the cellular region. By so neglecting possible variations due to the local composition of the cytological material (for example depending on the local fractions of fibers and cytosol), this (averaged) modulus can be considered homogeneous over the cell, the stiffness heterogeneity of the cytoplasm being thus attributed to its equivalent height. Under this hypothesis, the term $\overline{E_c\, A_c}$ has been estimated by exploiting the mechanical AFM data outside the nuclear zone, where the AFM tip only encounters the cell medium. More precisely, outside the nucleus, say $\mathcal{I}^{out,j} = \mathcal{I}_1^{out,j} \cup \mathcal{I}_2^{out,j} = \{s \in \left[s_1^{(j)}, s_n^{(j)} - \tilde{b}_n^{(j)}\right] \cup \left[s_n^{(j)} + \tilde{b}_n^{(j)}, s_2^{(j)}\right]\}$, one can obtain engineering estimations of the stiffness and height parameters as

$$\overline{K}_c^{out,j} = \frac{1}{2}\left[\frac{1}{(s_n^{(j)} - \tilde{b}_n^{(j)}) - s_1^{(j)}} \int_{\mathcal{I}_1^{out,j}} K_{AFM}^{(j)}(s)\, ds + \frac{1}{s_2^{(j)} - (s_n^{(j)} + \tilde{b}_n^{(j)})} \int_{\mathcal{I}_2^{out,j}} K_{AFM}^{(j)}(s)\, ds \right] \tag{S.8}$$

$$\overline{h}_c^{out,j} = \frac{1}{2}\left[\frac{1}{(s_n^{(j)} - \tilde{b}_n^{(j)}) - s_1^{(j)}} \int_{\mathcal{I}_1^{out,j}} f_{c/0}^{(j)}(s)\, ds + \frac{1}{s_2^{(j)} - (s_n^{(j)} + \tilde{b}_n^{(j)})} \int_{\mathcal{I}_2^{out,j}} f_{c/0}^{(j)}(s)\, ds \right] \tag{S.9}$$

In such a way one finds $\overline{E_c\,A_c} = \overline{K}_c^{out,j}\,\overline{h}_c^{out,j}$, while the combination of Eqs. (S.5)-(S.9) let to evaluate the nucleus stiffness and the cytoplasm stiffness for the j-th projection as

$$\overline{K}_c^{int,j} = \frac{\overline{E_c\,A_c}}{\overline{h}_c^{int,j}}, \tag{S.10}$$

$$\overline{K}_c^{out,j} = \frac{\overline{E_c\,A_c}}{\overline{h}_c^{out,j}}, \tag{S.11}$$

$$\overline{K}_n^{j} = \overline{K}_{nc}^{int,j}\left[1 - \frac{\overline{K}_{nc}^{int,j}}{\overline{K}_c^{out,j}}\frac{\overline{h}_c^{int,j}}{\overline{h}_c^{out,j}}\right]^{-1} \tag{S.12}$$

At last, the engineering estimation for spring constants in the structural paradigm can be obtained through a geometric mean of the stiffness (S.10) derived along the two (or p, in general) projections, i.e.

$$\begin{aligned}
\overline{K}_c^{int} &= \sqrt[p]{\prod_{j=1}^{p}\overline{K}_c^{int,j}}, \\
\overline{K}_c^{out} &= \sqrt[p]{\prod_{j=1}^{p}\overline{K}_c^{out,j}}, \\
\overline{K}_n &= \sqrt[p]{\prod_{j=1}^{p}\overline{K}_n^{j}},
\end{aligned} \tag{S.13}$$

A synoptic scheme of the algorithm has been reported for convenience in figure S3. Analyses performed on DU145 tumor cells and non-tumoral PNT1A cells –the most representative sample of tumor and healthy cells for which complete height and stiffness maps were acquired to obtain robust information– returned nuclear stiffness values of 7.44 ± 4.10 mN/m and 15.06 ± 1.89 mN/m for the two cell types, while the outer environmental stiffness measured 2.87 ± 0.17 mN/m and 13.5 ± 1.87 mN/m. The computed peri-nuclear cytoskeleton stiffness values were instead 7.65 ± 5.0 mN/m and 18.25 ± 3.39 mN/m. These data overall confirm the mechanical differences between cancer and healthy cells already present in literature (1). Interestingly, DU145 cells exhibited much wider variability, some of these cells exhibiting a softer peri-nuclear medium with respect to other ones (4.11 ± 1.5 mN/m and 11.19 ± 1.36 mN/m), this difference potentially contributing to produce distinct in frequency sensitivity that affect cell vibration and the related activation of biochemical pathways observed in biological experiments. Similarly, the post-processing of morphological data let to readily evaluate cell sizes and estimate nuclei volumes, finding equivalent radii of 3.45 ± 0.3 and 4.5 ± 0.9 μm for normal and tumor cell types with a mean nucleus-to-cytoplasm ratio of 0.47 and 0.65, respectively. This agrees with observations reporting that cancer cell nuclei appear more swollen due to the less structured nucleoplasm(2). Reliability of the predicted nucleus dimensions has been also assessed from reference fluorescence microscopy images of cultured cells. From geometric values, the mass terms of the nucleus as well as of the peri-nuclear and outer cytoplasm –respectively denoted as m_n, m_c^{in} and m_c^{out}– have been lastly calculated from volume integrals of cells' orographic scans and by attributing water density to the cytoplasm, while differences in density values for the nuclei of tumor and healthy cells have been taken into account according to literature evidence (2; 3).

In-frequency response of normal and cancer cells

When irradiated by ultrasounds, cells adhering on the Petri bottom vibrate as submerged in the liquid medium with an imposed ground acceleration (see Figure 1E). As reported in Figure 1F, the simplest but most effective mechanical paradigm to investigate the possible effects produced by the relative vibration of cell cyto-structure (CSK) and nucleus (NUC) under US stimulation on the basis of the available morpho-mecanical data can be constituted by a two degree-of-freedom (2-DOF) system. Both the DOFs have been modelled as Zener viscoelastic elements. In particular, the first DOF (the relative CSK displacement u_1) is representative of the portion cytoskeleton and cytoplasm structures involved into oscillation with effective (total) stiffness k_c and damping c_1, say the participating mass m_c of the extra-nuclear cell that neglects the spread adherent portion of the cell on the substrate. The second DOF u_2 instead refers to the nucleus of mass m_n, modelled as an in series element to account for its vibration inside the intra-cellular environment, which is mediated by an overall stiffness k_n and a damping c_2. For the sake of simplicity, one assumes that the effective stiffness constants of the cytoskeleton and the nucleus are partitioned in the purely elastic spring and the Maxwell's visco-elstic spring of each stage as $\beta_j\,k_j$ and $(1-\beta_j)\,k_j$ (with $j = \{c, n\}$ and $\beta_i \in \{0, 1\}$), respectively. This cell paradigm is supposed to undergo small oscillations and a ground acceleration $\ddot{u}_0$ is considered to model the US excitation. Importantly, cell oscillations are not in unconstrained conditions. Indeed, for the in vitro experiments at hand, cells adhere to the rigid bottom of the Petri dish and they are submerged into a shallow stratum of culture medium, in which ultrasounds propagate by slightly attenuating towards the free-surface. In this situation, the idealized cell structure has to

vibrate by accounting also for the movement of an overlying column of water-like liquid, which can affect the in frequency behavior of the system in the form an extracellular added-mass that exerts a force on the cell body proportional to the relative acceleration between the cell and the liquid-air interface. Such a contribution has been taken into proper account by considering an inerter type element with mass M_w (4). Also, a damper with constant c_w is considered to include water viscous contribution. Under these conditions, the free-body diagrams for the two DOF lead to the following equilibrium equations:

$$\begin{cases} F_{e2} + F_{v2} - F_{e1} - F_{v1} - F_{Mw} - F_{vw} & = m_c\,(\ddot{u}_0 + \ddot{u}_1) \\ -F_{e2} - F_{v2} & = m_n(\ddot{u}_0 + \ddot{u}_2) \end{cases} \tag{S.14}$$

where u_0 is the imposed ground displacement (dots indicate time derivative), $u_i, i \in \{1,2\}$ instead denote the degree of freedom of the cytoplasm mass m_c and the nucleus mass m_n, F_{ei} and F_{vi} are respectively the force of the elastic spring and of the Maxwell type viscoelastic element for the i-th standard linear solid stage, while F_{Mw} and F_{vw} indicate the inertial and viscous forces counteracting the unconstrained oscillations due to the overlying mass M_w of liquid medium.

By focusing first on the equation (S.14)$_1$ involving the mass m_c, constitutive equations let to write:

$$\begin{aligned} -k_{e1}\,u_1 - k_{v1}\int_0^\infty \dot{u}_1(s)\,e^{-\frac{k_{v1}}{c_1}(t-s)}\,ds + k_{e2}(u_2-u_1) + k_{v2}\int_0^\infty (\dot{u}_2(s)-\dot{u}_1(s))\,e^{-\frac{k_{v2}}{c_2}(t-s)}\,ds + \\ - M_w\,[\ddot{u}_f - \ddot{u}_1] - c_w\,[\dot{u}_f - \dot{u}_1] = m_c\,(\ddot{u}_1 + \ddot{u}_0) \end{aligned} \tag{S.15}$$

where u_f denotes the motion of the free-surface of water medium, while the stiffness elements have been conveniently indicated in this 2-DOF scheme as $k_{e1} = \beta_c\,k_c$, $k_{v1} = (1-\beta_c)\,k_c$ and $k_{e2} = \beta_n\,k_n$, $k_{v2} = (1-\beta_n)\,k_n$. Passing to the frequency domain with angular frequency ω one has(5)

$$\begin{aligned} -k_{e1}\,U_1 - k_{v1}(-j\omega)\frac{\tau_1}{1-j\omega\,\tau_1}\,U_1 + k_{e2}\,(U_2-U_1) + k_{v2}(-j\omega)\frac{\tau_2}{1-j\omega\,\tau_2}\,(U_2-U_1) + \\ - M_w\,(-\omega^2)\,[U_f - U_1] - c_w(-j\omega)\,[U_f - U_1] = -\omega^2\,m_c\,(U_1+U_0) \end{aligned} \tag{S.16}$$

In order to correlate the relative movement water free-surface with respect to the object vibration, one can consider that the ultrasound pressure wave (say p) in a medium propagates by attenuating along the propagation direction according to the attenuation law:

$$p(x) = p_0\,e^{-\alpha\,x}, \quad p = Z\,\dot{u} \tag{S.17}$$

where α is the attenuation coefficient and Z is the acoustic impedance. For the case at hand, by denoting with h the height of the water medium, one obtains the relation:

$$\dot{u}_f = \dot{u}_1\,e^{-\alpha\,h} \tag{S.18}$$

in which the height of the adherent cell is considered negligible with respect to that of the fluid column. Such a relation well approximates the dynamics of a fluid column subjected to free-surface conditions. Also, the used US transducers and the applied frequencies (from kHz to MHz) ensure a near field propagation with negligible dispersion due to beam divergence. Writing also the acceleration by means of a time-derivative of eq. (S.18) and by inserting it into (S.16), one obtains:

$$\begin{aligned} -k_{e1}\,U_1 - k_{v1}(-j\omega)\frac{\tau_1}{1-j\omega\,\tau_1}\,U_1 + k_{e2}\,(U_2-U_1) + k_{v2}(-j\omega)\frac{\tau_2}{1-j\omega\,\tau_2}\,(U_2-U_1) + \\ - M_w\,(-\omega^2)\left[e^{-\alpha\,h}-1\right]\,U_1 - c_w(-j\omega)\left[e^{-\alpha\,h}-1\right]\,U_1 = -\omega^2\,m_c\,(U_1+U_0) \end{aligned} \tag{S.19}$$

Given the shallow stratum of water as well as, in general, the reduced value of the absorption coefficient for the water at the frequency of interest, one can approximate the exponential absorption law to the first order by finding

$$\begin{aligned} -k_{e1}\,U_1 - k_{v1}(-j\omega)\frac{\tau_1}{1-j\omega\,\tau_1}\,U_1 + k_{e2}\,(U_2-U_1) + k_{v2}(-j\omega)\frac{\tau_2}{1-j\omega\,\tau_2}\,(U_2-U_1) + \\ - \alpha\,h\,M_w\,\omega^2\,U_1 - j\omega\,c_w\,\alpha\,h\,U_1 = -\omega^2\,m_c\,(U_1+U_0) \end{aligned} \tag{S.20}$$

To get non-dimensional quantities, let us divide the equation by the term $k_{e1}\,U_0$. By identifying the ratio $U_i/U_0 = H_i$ as the transfer function of the i-th degree of freedom, and by further introducing the following positions

$$\begin{aligned} &\sqrt{\frac{k_{e1}}{m_c}} = \omega_1^2, \quad \frac{k_{mi}}{k_{e1}} = \rho_{m\,i}, \quad \text{with} \quad m = \{e,v\} \quad \text{and} \quad i = \{1,2\} \\ &\Omega = \frac{\omega}{\omega_1}, \quad \overline{\tau}_i = \tau_i\omega_1, \quad \xi_w = \alpha\,h\,\frac{M_w}{m_c}, \quad \zeta_w = \alpha\,h\,\frac{c_w\omega_1}{k_{e1}} \end{aligned} \tag{S.21}$$

some algebraic passages lead to

$$-H_1\left[(1+\rho_{e1})+\rho_{v1}\frac{(-j\Omega\,\overline{\tau}_1)}{1-j\Omega\,\overline{\tau}_1}+\rho_{v2}\frac{(-j\Omega\,\overline{\tau}_2)}{1-j\Omega\,\overline{\tau}_2}\right]+H_2\left[\rho_{e2}+\rho_{v2}\frac{(-j\Omega\,\overline{\tau}_2)}{1-j\Omega\,\overline{\tau}_2}\right]+$$
$$-\Omega^2\xi_w\,H_1-j\Omega\,\zeta_w\,H_1=-\Omega^2\,[1+H_1] \tag{S.22}$$

With similar passages and by employing the same positions (S.21), the second equation $(S.14)_2$ describing the vibration of the internal nucleus m_n can be re-arranged by giving:

$$\left[\rho_{e2}-\rho_{v2}\;\frac{j\Omega\,\overline{\tau}_2}{1-j\Omega\,\overline{\tau}_2}\right](H_1-H_2)=-\Omega^2\,\mu\,(1+H_2) \tag{S.23}$$

in which $\mu=m_n/m_c$ is the ratio between the nucleus mass and the mass of the participating cellular structures. Equations (S.22) and (S.23) then return the harmonic response of an isolated cell adhering on a Petri dish and they have been particularized by uploading the cell-specific parameters estimated from processing the morpho-mechanical data obtained through AFM tests. In order to then attribute to the mechanical components of the present model values consistent with the overall properties obtained by AFM investigations, one has to somehow identify the elastic stiffness and the damping coefficient of the elements. The values of c_i have been set starting from literature data (6), while the coefficients related to the culture medium are calculated from observations of the experimental setup and by means of well-established literature values related to the US propagation in water. On the other hand, we need to properly identify the elastic and morphological features of the present dynamic model by starting from the above discussed AFM outcomes. In doing this, since cultured cells appear spread in large portion on the substrate with high width-to-height ratio, it is reasonable to assume that adhesion and overlying liquid weight prevent part of the CSK mass to actively participate to the oscillation by producing marked displacement variations in its elements. For this reason, the cytoskeletal mass m_c is written as $m_c=\lambda\,(m_c^{in}+m_c^{out})$, where λ is a participating mass coefficient assumed to vary in the interval $\lambda\in\{\lambda_n,1\},\quad \lambda_n=m_c^{in}(m_c^{in}+m_c^{out})^{-1}$ and introduced to account for the variability of the cellular mass effectively contributing to the vibration with respect to the part that adheres on the substrate by not determining relevant dynamic effects. Accordingly, the nucleus stiffness of the dynamic model can be identified as $k_n=\overline{K}_n$ while the CSK stiffness term is estimated by resorting to the weighted Voigt-type relation $k_c=\overline{K}_c^{int}+(\lambda-\lambda_n)\,\overline{K}_c^{out}$, thus returning the elastic constants of the viscoelastic elements k_{ei} and k_{vi} when supposing an equal partition between elastic and viscous components (the values $\beta_i=1/2$ have been adopted without loss of generality). With these positions and upon considering common values for damping coefficient of cell components, cell-specific transfer functions can be obtained from solving (S.22) and (S.23) in order to obtain theoretical predictions of help for calibrating the US sonication experiments implemented on cells by using the US equipment reported in Fig. S1.

Supplementary Figures

Supplementary Figure 1

A. Scheme of the ultrasound treatment protocol. **B**. Implementation of the actual US station used for experiments.

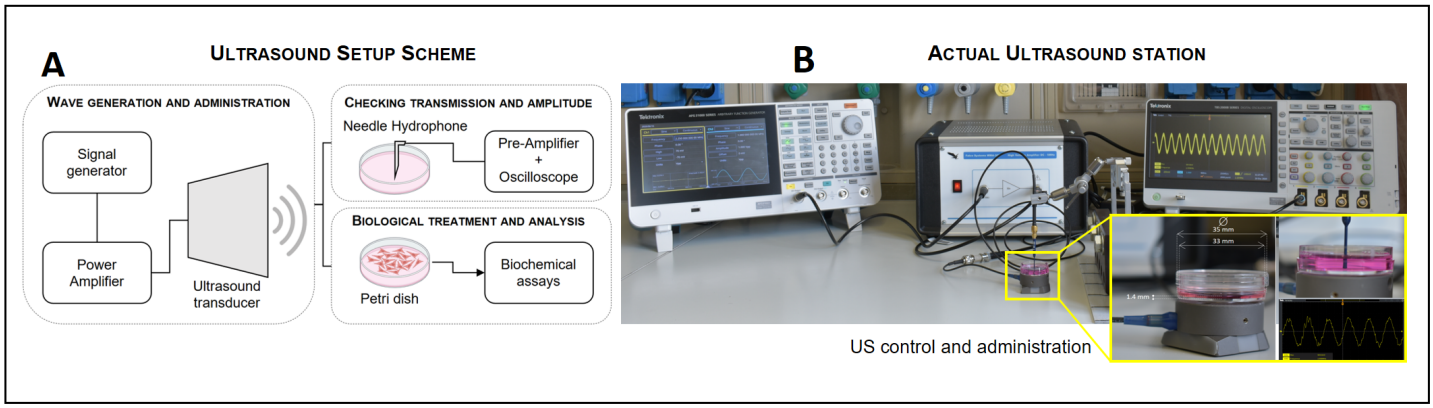


Figure S1

Supplementary Figure 2

Stiffness spectra of prostate tumoral and non-tumoral cells obtained via AFM scanning, showing that VCAP and DU145 cancer cell types exhibit reduced stiffness with respect to BPH1 and PNT1A cells (controls).

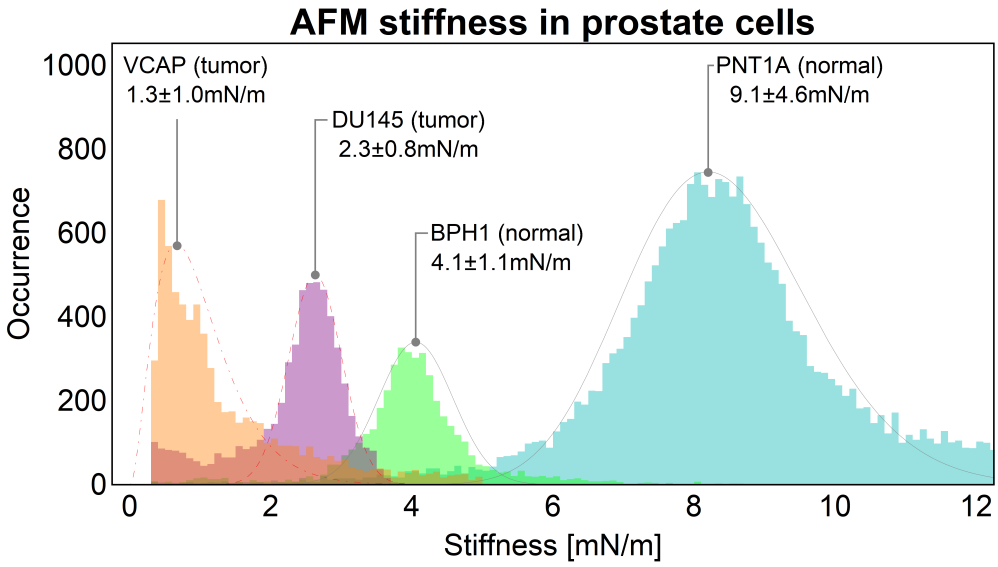


Figure S2

Supplementary Figure 3

Flow chart illustrating the combined morpho-mechanical identification of cell properties obtained from AFM measurements.

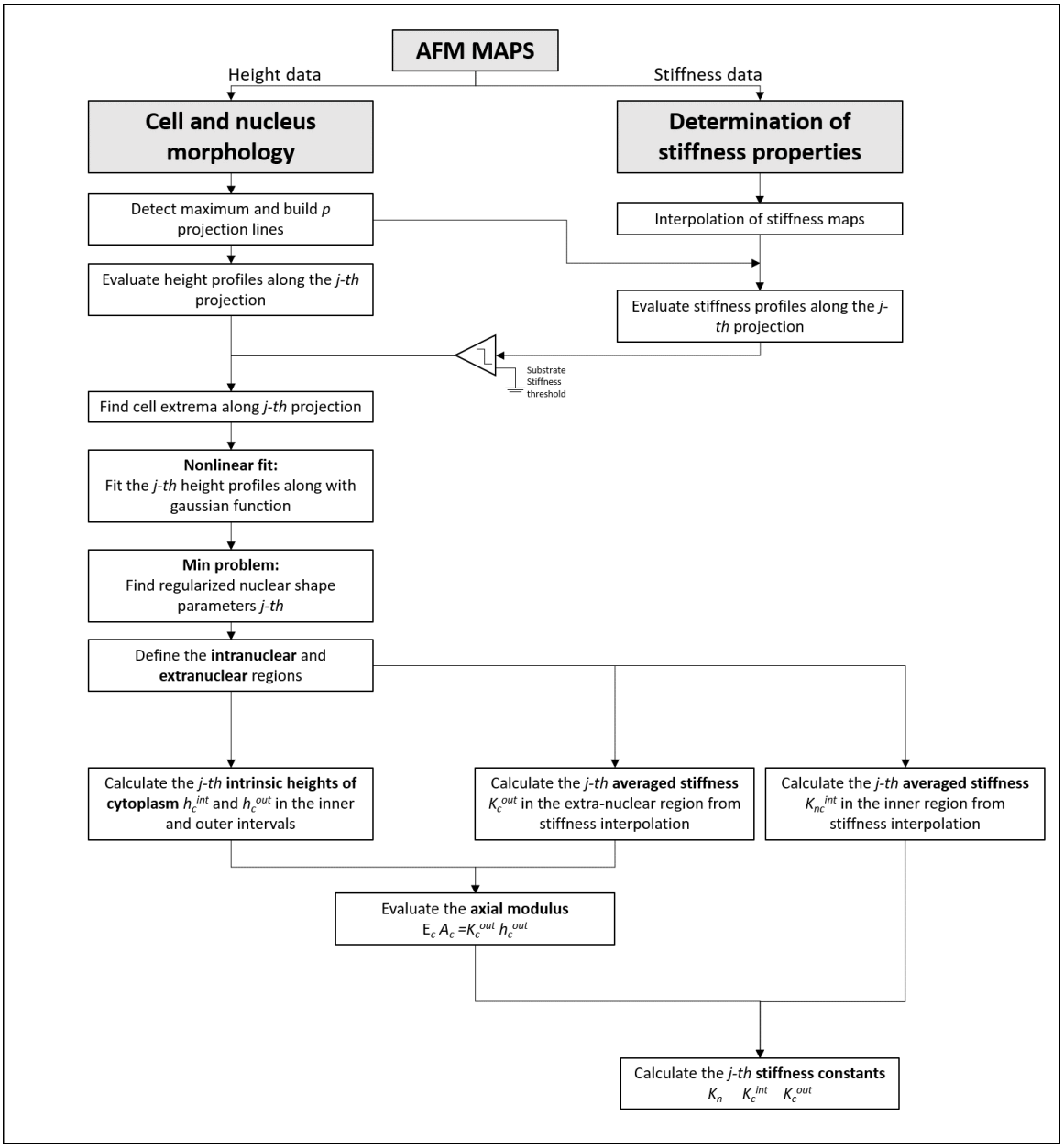


Figure S3

Supplementary Figure 4

A. Growth curves of BPH1 and PNT1A treated or not with 1 MHz LITUS for 20 min and counted at the indicated time points (hours). Data are the mean ± SD of a single experiment performed in duplicate. **B.** Growth curves of DU145, LNCaP and VCap treated or not with 1 MHz LITUS for 20 min and counted at the indicated time points (hours). Data are the mean ± SD of a single experiment performed in duplicate. p * <0,05; ** < 0,01; *** < 0,001. **C.** bar graph representing the number of the indicated cell lines counted after a single treatment (1) or repeated treatments (4, one treatment every 12 hours for four times) with 1 MHz LITUS (20 min). Each dot represents a different count. Two independent experiments were performed in duplicate.

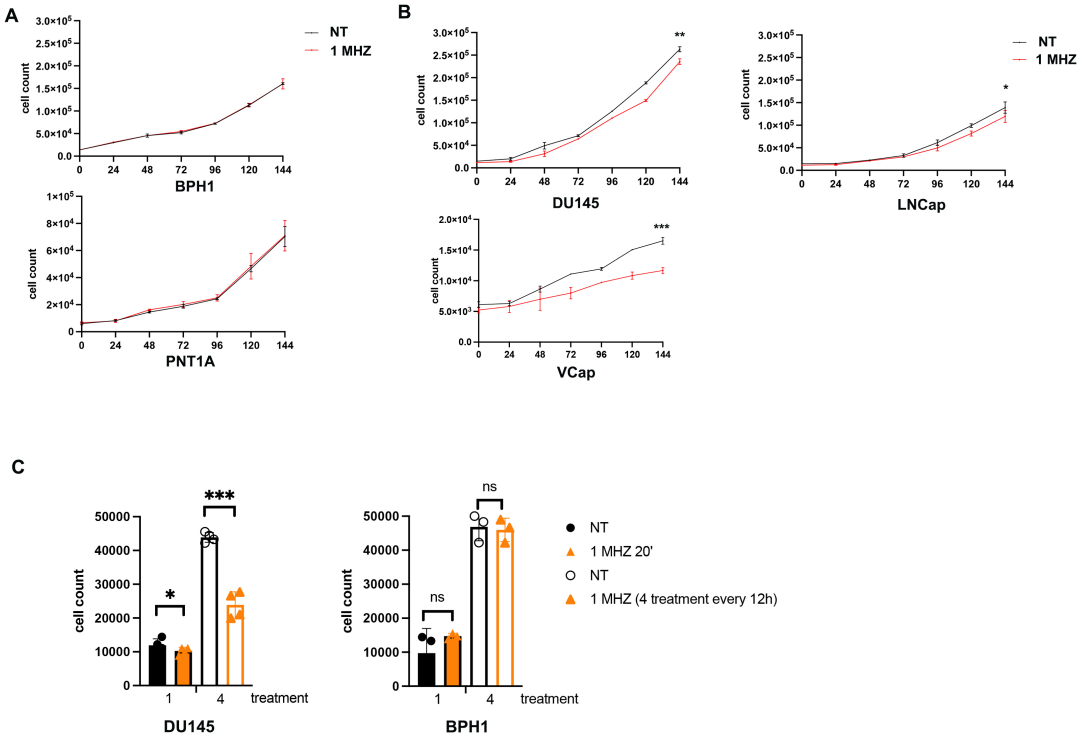


Figure S4

Supplementary Figure 5

A. Related to Fig. 2. 2X magnification of cells indicated in Figure 2C showing immunofluorescence staining of Tubulin. The indicated cell lines were treated or not with 1 MHz LITUS. After 20' of sonication cells were fixed and stained with anti-Tubulin antibody (green signal) and DAPI (blue signal). **B.** Left: Representative images of confocal immunofluorescence of the indicated cell lines treated or not with 1 MHz LITUS. After 20 min of sonication, cells were fixed and subjected to immunofluorescence with anti-Tubulin antibody (green signal) and DAPI (blue signal). Right: Cells showing abnormal Tubulin signal were counted and represented as the percentage of the total number of cells observed in each field. Three independent experiments were performed. Scale bar 10 μm.

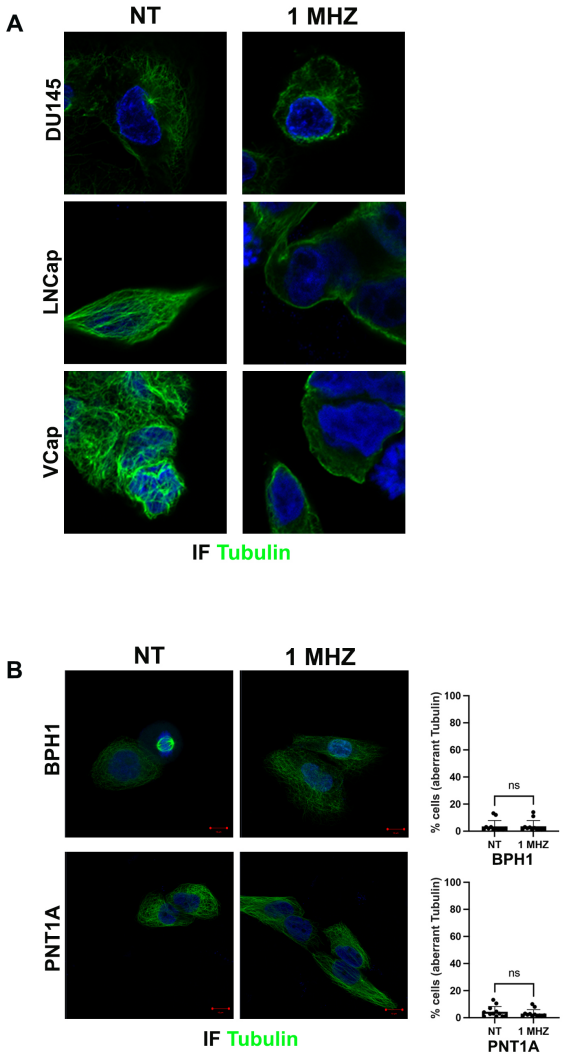


Figure S5

Supplementary Figure 6

A. Related to Fig. 3. 2X magnification of cells indicated in Figure 3A showing immunofluorescence staining of Lamin A/C. The indicated cell lines were treated or not with 1 MHz LITUS. After 20' of sonication cells were fixed and stained with anti-Lamin A/C (red signal) and DAPI (blue signal). **B.** Left: Representative images of confocal immunofluorescence of the indicated control cell lines (BPH1 and PNT1A treated or not for 20 min with 1 MHz LITUS). Right: Cells showing aberrant Lamin A/C signal were counted and represented as the percentage of the total number of cells observed in each field. Each dot represents a different field. Three independent experiments were performed. Scale bar 10 μm. **C.** On the left: bar graphs representing the indicated nuclear descriptor parameters (perimeter and round shape) obtained in DU145 subjected to indirect immunofluorescence with anti-Lamin A/C antibody. Cells were treated or not with 1 MHz LITUS 20' and immediately fixed. Each dot represents a different measurement. At least 50 nuclei were measured. On the right: 3D reconstruction of the nuclear Lamina A/C in BPH1 treated or not with 1 MHz LITUS. **D.** On the left: bar graphs representing the indicated nuclear descriptor parameters (perimeter and round shape) obtained in BPH1 subjected to indirect immunofluorescence with anti-Lamin A/C antibody. Cells were treated or not with 1 MHz LITUS 20' and immediately fixed. Each dot represents a different measurement. At least 50 nuclei were measured. On the right: 3D reconstruction of the nuclear Lamina A/C in BPH1 treated or not with 1 MHz LITUS. **p $<$ 0.01; ****p $<$ 0.0001.

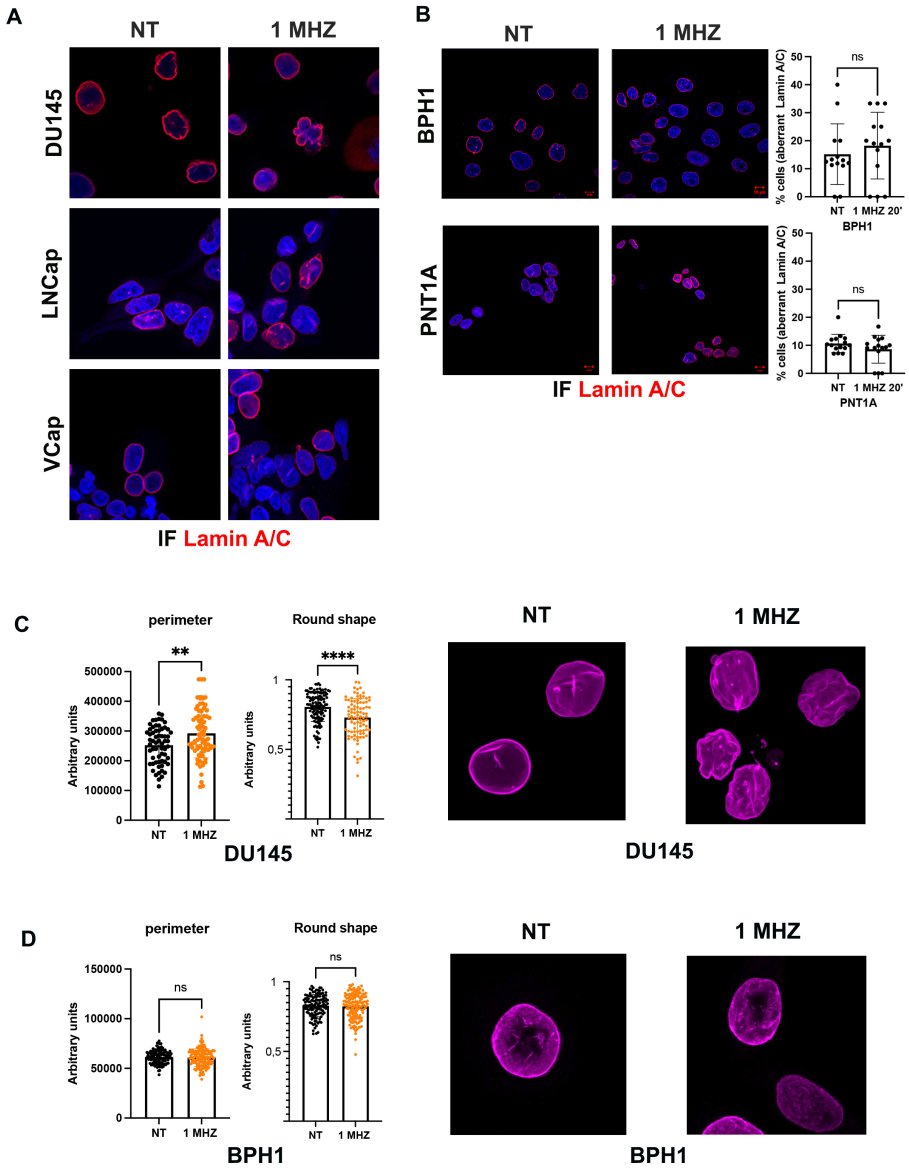


Figure S6

Supplementary Figure 7

A and **B**. Representative confocal immunofluorescence images of BPH1 (**A**) and DU145 (**B**) cells treated or not with 1 MHz LITUS. After 20 min of sonication, cells were fixed and subjected to immunofluorescence with anti-Lamin B (red signal) and DAPI (blue signal). Cells showing aberrant Lamin B were counted and plotted as % of the total number of cells counted in each field. Each plot represents a different field. Three independent experiments were performed. Scale bar 10 μm. **C.** Representative confocal immunofluorescence images of DU145 stably expressing H2B-GFP plasmid, treated or not with 1 MHz ultrasounds. After 20 min of sonication, cells were fixed and subjected to immunofluorescence with anti-Lamin A/C (red signal) and DAPI (blue signal). Cells showing aberrant Lamin A/C were counted and plotted as % of the total number of cells counted in each field. Each plot represents a different field. Three independent experiment were performed. Scale bar 10 μm. **p < 0.01. ****p < 0.0001.

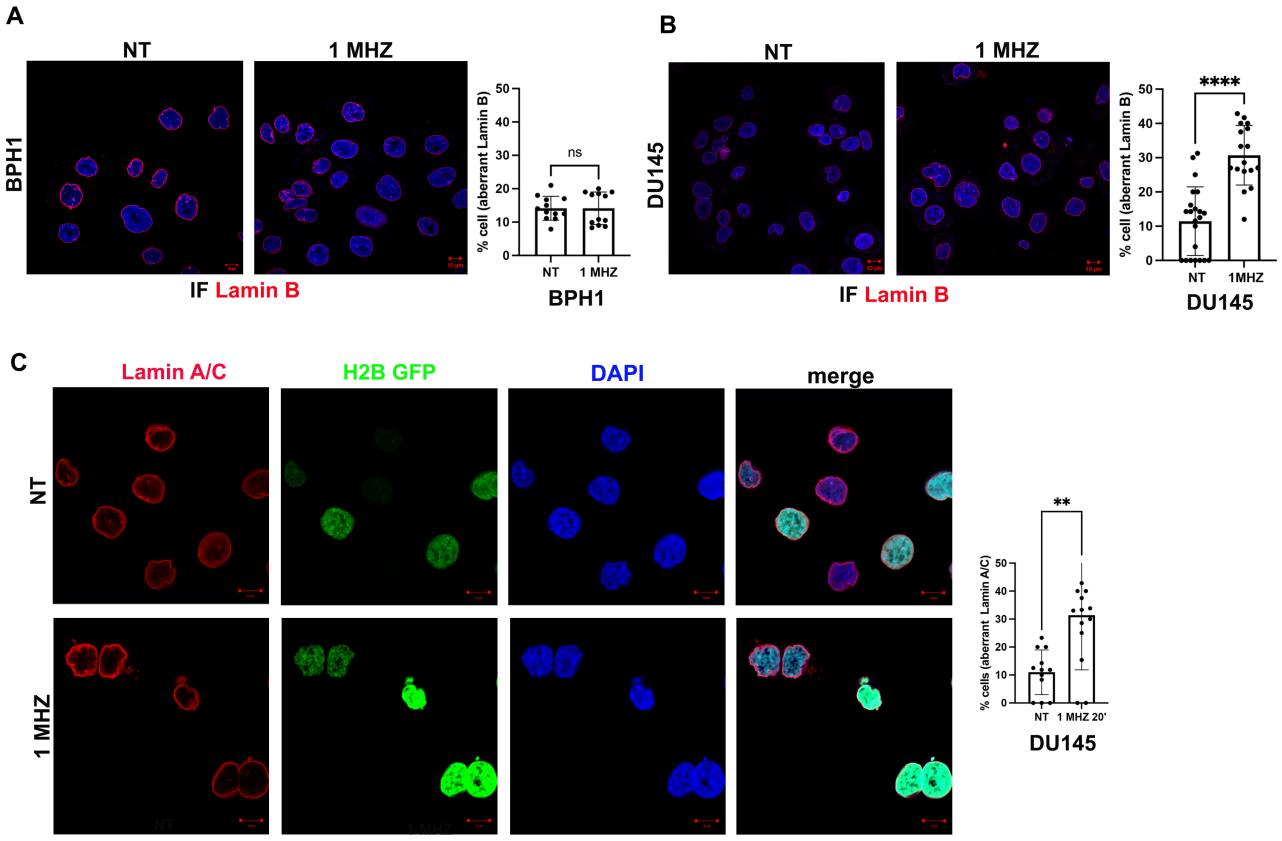


Figure S7

Supplementary Figure 8

A. Left: Representative images of confocal immunofluorescence of the indicated cell lines treated or not with 1 MHz ultrasounds. After 6 hours from sonication, cells were fixed and subjected to confocal immunofluorescence with anti-γH2AX (green signal) and DAPI (blue signal). Right: The number of γH2AX signal (foci) per nucleus were counted and represented as a dot in the graph shown. Three independent experiments were performed. Scale bar 10 μm. **B.** Left: representative images of confocal immunofluorescence of BPH-1 and DU145 cells treated or not with 1 MHz LITUS for 20 min. After 6h from sonication, cells were fixed and subjected to immunofluorescence with anti-53BP1 (green signal) and DAPI (blue signal). Right: The number of 53BP1 nuclear signal (foci) in BPH1 and DU145 treated as described in (A). **C.** Left: representative confocal immunofluorescent images of DU145 cells treated or not with 1 MHz ultrasounds. Immediately (T0) or after 6h (T 6h) from sonication, cells were fixed and subjected to immunofluorescence with anti-γH2AX (green signal) and Lamin A/C (red signal) antibodies and counterstained with DAPI (blue signal). For each condition pictures at higher magnification are shown in lower panels; scale bar 10 μm. Right: bar graph representing the number of γH2AX nuclear foci in treated cells showing or not aberrant Lamin A/C signal. DU145 cells were treated as described in (C left). *p $<$ 0.05; **p $<$ 0.01; ***p $<$ 0.001; ****p $<$ 0.0001.

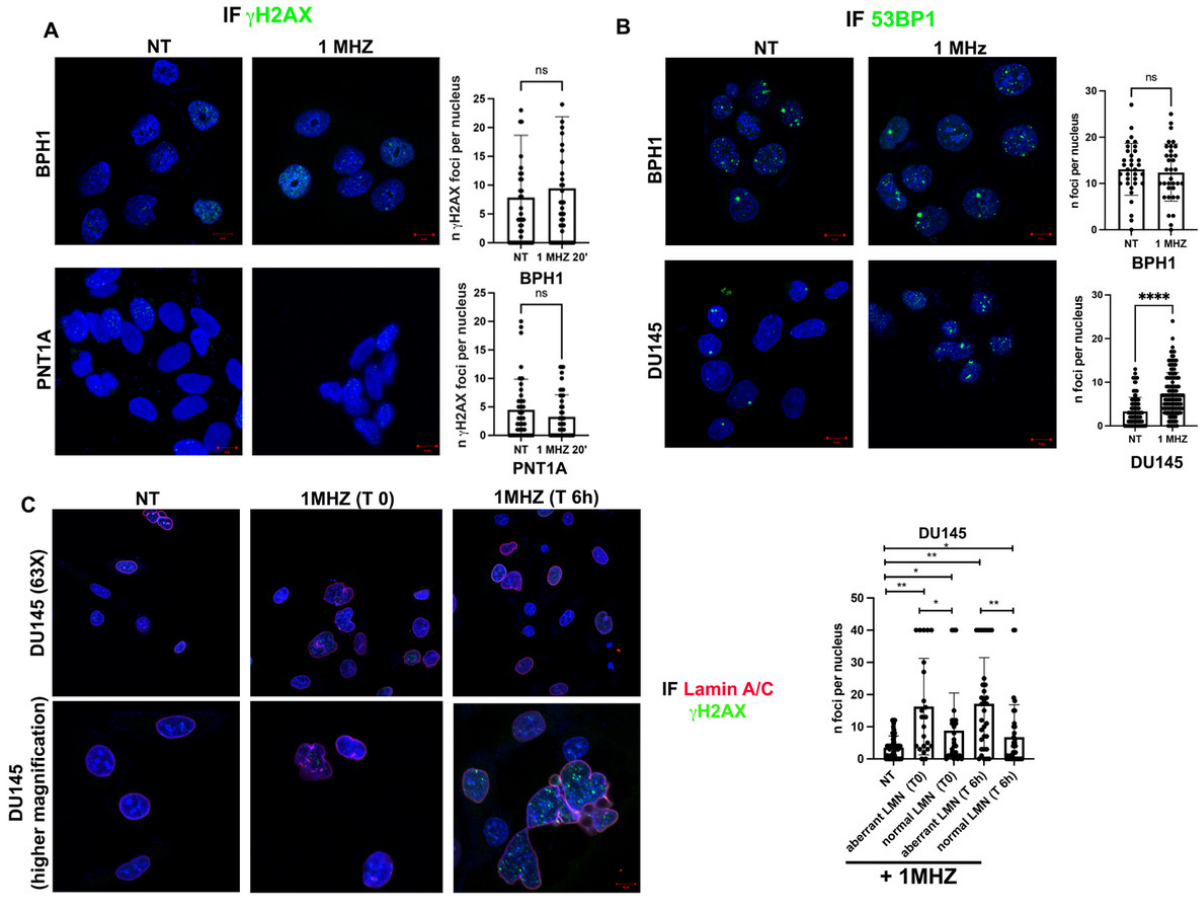


Figure S8

Supplementary Figure 9

A. Left: bar graph representing the number of γH2AX foci counted in DU145 cells showing a round lamina or an aberrant lamina (cells showing a Lamin A/C signal with at least one bleb). DU145 cells were transfected with Lamin A/C mCherry reporter. After 48h were treated or not with 1 MHz LITUS. After 20 min of sonication, cells were fixed and subjected to immunofluorescence with anti-γH2AX (green signal) and DAPI (blue signal). Fifteen different cells showing aberrant or round lamina were considered. Right: representative confocal immunofluorescent images of DU145 transfected with Lamin A/C mCherry reporter and treated as described in A; scale bar 10 μm. **B.** Left: bar graph representing the number of 53BP1 foci counted in DU145 cells showing a round lamina or an aberrant lamina (cells showing a Lamin A/C signal with at least one bleb). DU145 cells were transfected with Lamin A/C mCherry reporter and treated or not with 1 MHz LITUS. After 20 min of sonication, cells were fixed and subjected to immunofluorescence with anti-53BP1 (green signal) and DAPI (blue signal). Fifteen different cells showing aberrant or round lamina were considered. Right: representative confocal immunofluorescent images of DU145 transfected with Lamin A/C mCherry reporter and treated as described in (B, left); scale bar 10 μm. *p $<$ 0.05; **p $<$ 0.01; ***p $<$ 0.001; ****p $<$ 0.0001.

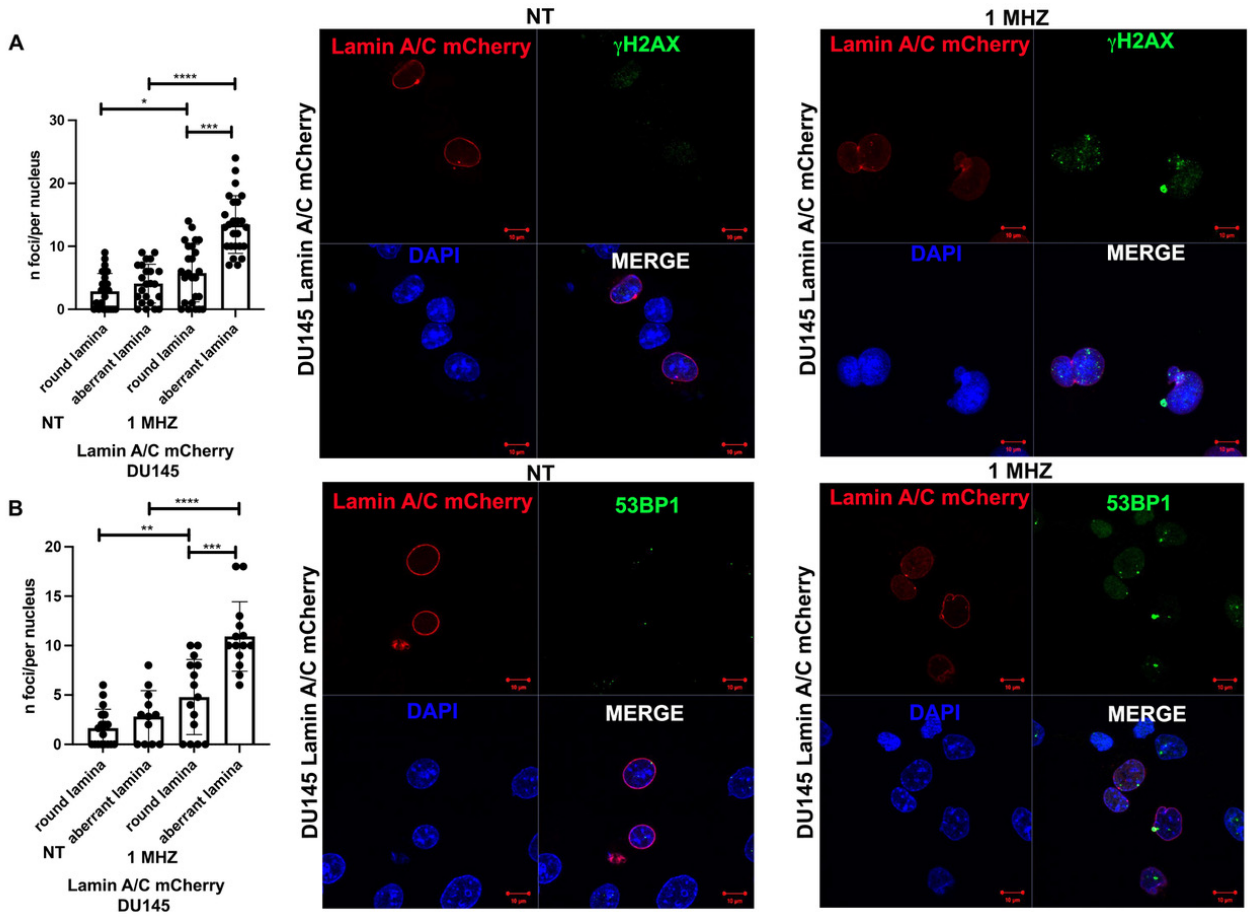


Figure S9

Supplementary Figure 10

A. Bar graph representing the percentage of cells displaying cGAS puncta in each field in untreated (NT) and LITUS-treated LNCap cells (20 min, 1 MHz). After 12h from treatment, cells were fixed and subjected to immunofluorescence with anti-cGAS. ****p $<$ 0.0001. **B.** Left: bar graph representing the percentage of cells showing cGAS accrual signal in cells carrying a round lamina or aberrant lamina (cells showing a Lamin A/C signal with at least one bleb). Right: representative confocal immunofluorescent images of DU145 transfected with Lamin A/C mCherry reporter treated or not with 1 MHz ultrasounds. Immediately after sonication, cells were fixed and subjected to immunofluorescence with anti-cGAS antibody (green signal) and counterstained with DAPI (blue signal); scale bar 10 μm.

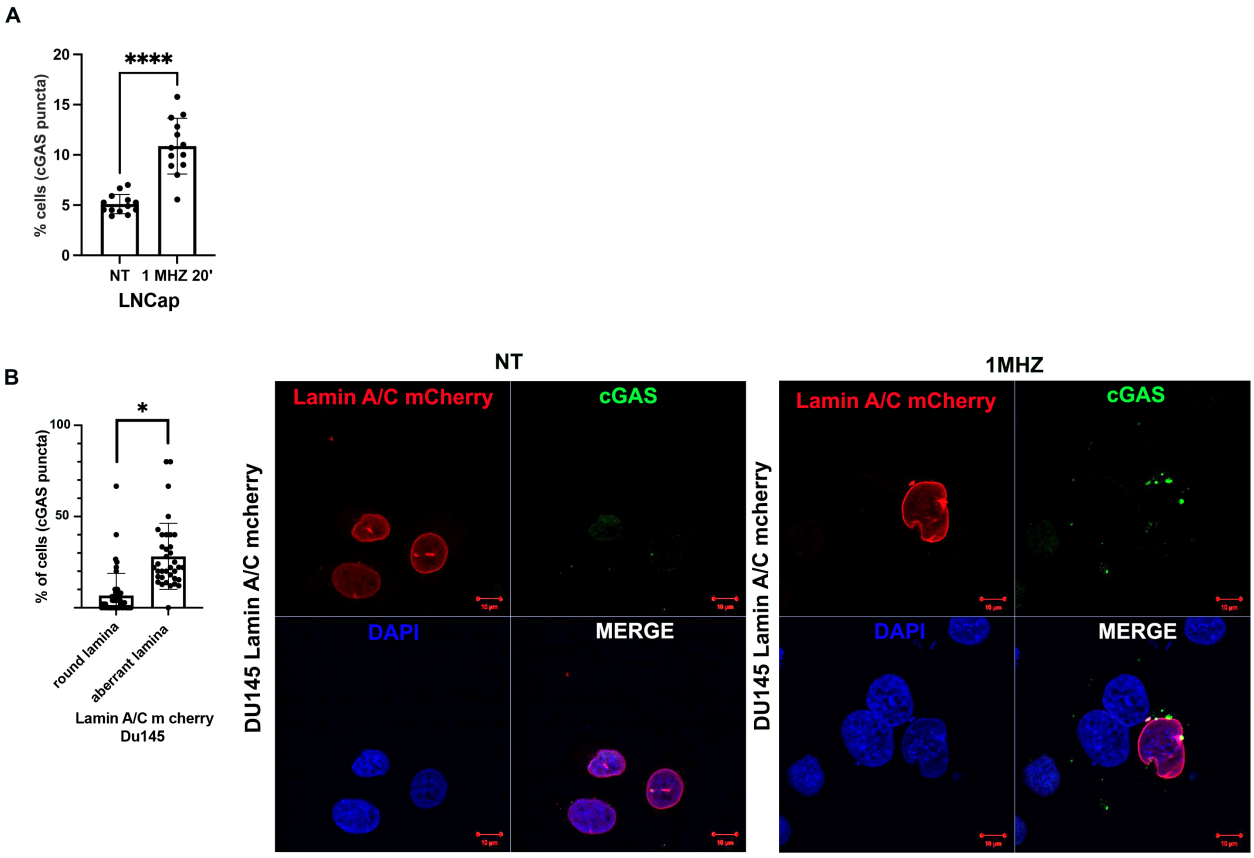


Figure S10

Supplementary Figure 11

A. Western blotting of SUN2 protein in DU145 transiently transfected with short interference (siRNA) against SUN2 (siSUN2) or control (siCTR). Tubulin was used as loading control. **B.** Representative images of γH2AX immunofluorescence in siCTR and siSUN2 treated DU145 cells. DU145 were transfected with siRNA control (siCTR) or against SUN2 (siSUN2). After 48h, cells were subjected to 1 MHz LITUS for 20 min, and after 6h cells were fixed and subjected to immunofluorescence with anti-γH2AX. Scale bar 10 μm. **C.** Representative images of cGAS immunofluorescence in siCTR and siSUN2 DU145 cells treated as described in (A). After 12h from treatment, cells were fixed and subjected to immunofluorescence with anti-cGAS. Scale bar 10 μm.

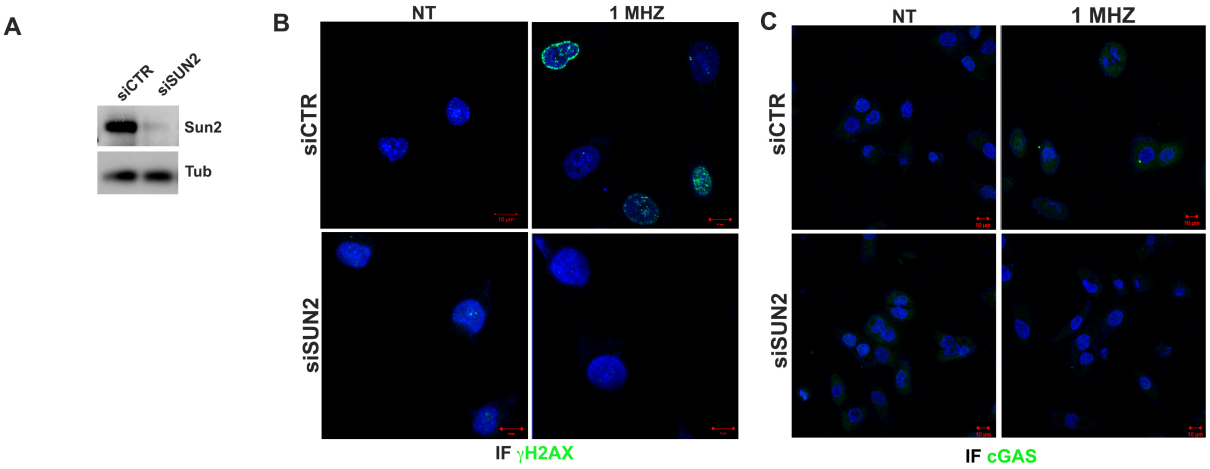


Figure S11

Supplementary Figure 12

A. BAF mRNA fold change in DU145 and BPH1 cells transfected with siRNA against BAF (siBAF) or siRNA control (siCTR), measured by RT-PCR compared to GAPDH expression. **B.** Representative images of Lamin A/C immunofluorescence in siCTR and siBAF DU145 cells. After 48h from transfection, cells were subjected to 1 MHz sonication, fixed and subjected to immunofluorescence. Scale bar 10 μm. **C.** Representative pictures of colony-formation assays of siCTR and siBAF cells treated or not with 1 MHz and grown for 12 days. Colonies were stained with crystal violet. **D.** Left: Representative images of Lamin A/C immunofluorescence in siCTR and siBAF BPH1 cells. After 48h from transfection, cells were subjected to 1 MHz sonication, fixed and subjected to immunofluorescence. Scale bar 10 μm. Right: bar graphs representing the percentage of cells showing aberrant Lamin A/C signal. Each dot represents a different field. **E.** Left: representative pictures of colony-formation assays of siCTR and siBAF cells treated or not with 1 MHz and grown for 12 days. Colonies were stained with crystal violet. Right: bar graph representing the number of colonies in each well. Each dot represents a single experiment plated in a single well. ***p $<$ 0.001.

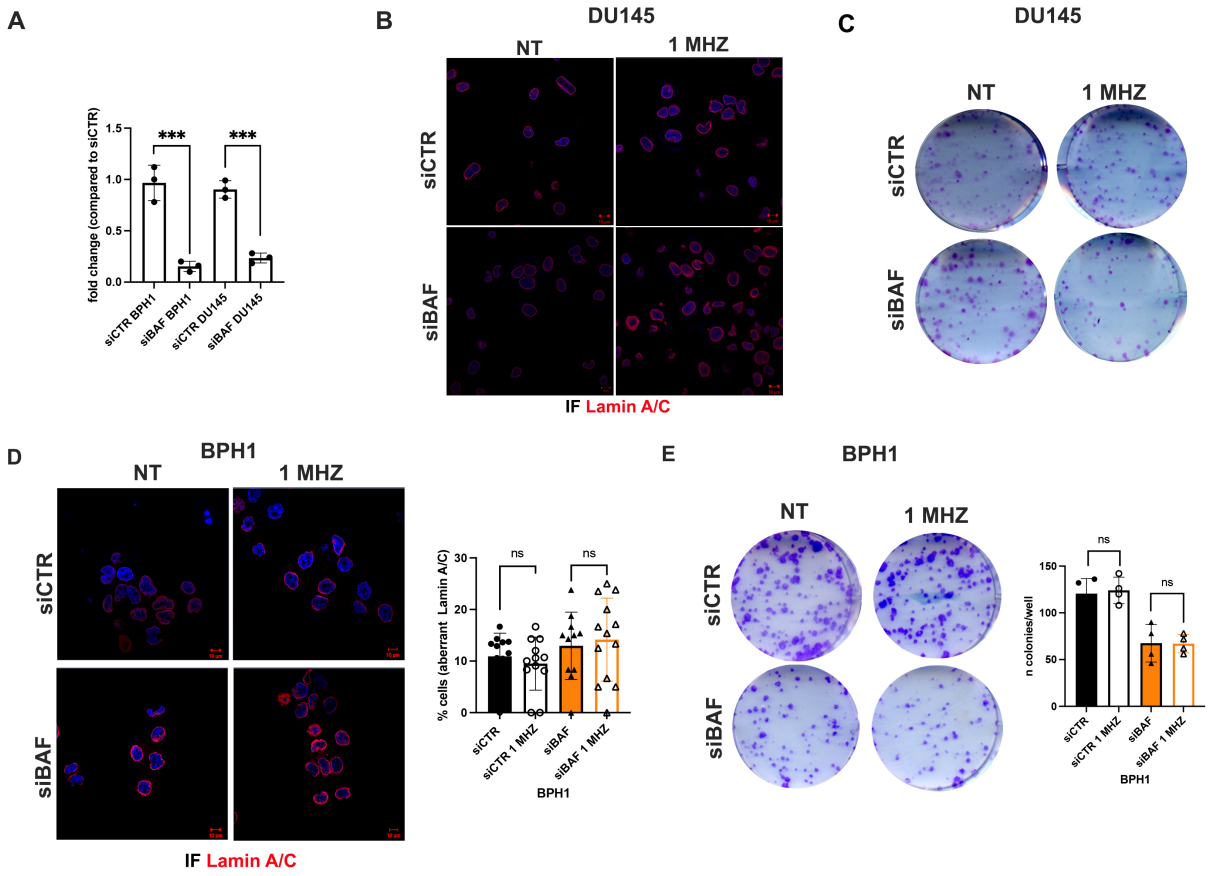


Figure S12

References

[1] Fraldi, M., Cugno, A., Deseri, L., Dayal, K., & Pugno, N. M. A frequency-based hypothesis for mechanically targeting and selectively attacking cancer cells. *J R Soc Interface*, **12** (111), 20150656 (2015).

[2] Lammerding, J. Mechanics of the nucleus. *Compr Physiol*, **1**(2), 783 (2011).

[3] Geltmeier, A., Rinner, B., Bade, D., Meditz, K., Witt, R., Bicker, U., ... & Maier, P. Characterization of dynamic behaviour of MCF7 and MCF10A cells in ultrasonic field using modal and harmonic analyses. *PloS one*, **10**(8), e0134999 (2015).

[4] Smith, M. C. Synthesis of mechanical networks: the inerter. *IEEE Trans Autom Control*, **47**(10), 1648-1662 (2002).

[5] W.H. Press, B.P. Flannery, S.A. Teukolsky, W.T. Vetterling, Numerical Recipes, Cambridge University Press Equation 12.01 p. 381 (1986).

[6] Tam, A. K., Mogilner, A., & Oelz, D. B. Protein friction and filament bending facilitate contraction of disordered actomyosin networks. *Biophys J*, **120**(18), 4029-4040 (2021).